Thin Solid Films 668 (2018) 14–22

Contents lists available at ScienceDirect

Thin Solid Films

journal homepage: www.elsevier.com/locate/tsf

Crack arrest in thin metallic film stacks due to material- and residual stress inhomogeneities

D. Kozic[a,*], H.-P. Gänser[a], R. Brunner[a], D. Kiener[b], T. Antretter[c], O. Kolednik[d]

[a] Materials Center Leoben Forschung GmbH, Leoben, Austria
[b] Department Materials Physics, Montanuniversität Leoben, Austria
[c] Institute of Mechanics, Montanuniversität Leoben, Austria
[d] Erich Schmid Institute of Materials Science, Austrian Academy of Sciences, Leoben, Austria

ARTICLE INFO

Keywords:
Thin metallic films
Local crack driving force
Residual stress
Finite element modeling
Material inhomogeneity
Fracture mechanics

ABSTRACT

Miniaturized materials, in general, exhibit higher strength compared to their bulk counterparts. As a consequence, their resistance to fracture is often compromised. However, the effect of material inhomogeneities can be used to significantly improve the fracture toughness of thin film components. In this work, the material inhomogeneity effect on the crack driving force, caused by material property and residual stress variations in thin tungsten and copper stacks, is numerically investigated. To this purpose, a finite element analysis is performed using the concept of configurational forces. In this way, we are able to distinguish between the various inhomogeneity effects and draw conclusions about the effective crack driving force. It is demonstrated that the material inhomogeneity effect is not solely determined by the material property variations at the interfaces, since an important contribution emerges due to a smooth residual stress gradient within the layers. The possibility to separate the different effects represents an opportunity for cost efficient design of future reliable thin film microelectronic components.

1. Introduction

Thin metallic films are commonly used for microelectronic applications. Following the trend of miniaturization, the film thickness is consistently decreasing along with the overall device dimensions. Concurrently, the strength of a material increases if either the grain size [1–4] or the size of single-crystalline volumes [5–11] is reduced. Recent investigations deal with the interplay of internal and external dimensions [12–15], which opens the possibility of tailoring the material's strength for specific applications. However, it is very important to note that an increased strength is in most cases accompanied by a decreased fracture toughness of the materials [16].

A crack in a material starts to propagate if the crack driving force equals or exceeds the fracture toughness of the material. The crack driving force is a loading parameter for the crack and depends on the load, the crack length and the geometry of the considered body [17]. It is easy to evaluate the crack driving force in homogeneous components. For inhomogeneous components, such as thin film stacks for microelectronic devices, the material inhomogeneity effect must be taken into account.

Imagine an externally loaded layered composite with a crack that lies in the vicinity of and perpendicular to an interface (IF). Depending on the properties of the involved materials, the crack driving force at a given load can either be larger or smaller compared to that of a homogeneous material. Crack growth is facilitated in the former case and the crack tip is said to feel an anti-shielding effect due to the material inhomogeneity. In the latter case crack propagation is hindered and the crack tip experiences a shielding effect. Anti-shielding occurs if the crack is about to propagate from a material with higher Young's modulus and/or higher yield strength into a material with lower modulus and/or strength. On the contrary, shielding occurs if the crack is approaching an IF to a material with higher Young's modulus and/or higher yield strength [18,19].

Microelectronic components incorporate various small-scale materials with a diversity of material properties. For example, multi-layer stacks are fabricated with alternating soft and hard thin films [20,21]. If the layers are appropriately arranged, the shielding effect can be utilized to arrest cracks in the soft interlayers and prevent their further propagation through the structure [22,23]. Such a strategy is in some cases inspired by natural structures [24–27]. For instance, deep sea sponges have a multi-layered structure consisting of a stiff and strong bio-glass matrix which incorporates thin and soft protein interlayers

* Corresponding author.
E-mail address: darjan.kozic@mcl.at (D. Kozic).

https://doi.org/10.1016/j.tsf.2018.10.014
Received 8 March 2018; Received in revised form 2 October 2018; Accepted 8 October 2018
Available online 10 October 2018
0040-6090/

serving as crack stoppers. In such materials the crack driving force is significantly decreased and the load necessary for further crack growth becomes very high as soon as the crack tip arrives in the soft layer. This means that the fracture toughness increases compared to a homogeneous material, without suffering a noticeable loss in stiffness or strength. The use of material property variations to improve the fracture properties of functional materials has been the topic of several investigations, see e.g. [26,28–34].

The same concept of shielding or anti-shielding can be applied for the effect of residual stresses in a body [35]. For instance, compressive residual stresses can be used to counter tensile stresses originating from external loading and have to be overcome before crack propagation is possible. Thin film components for microelectronic applications are most commonly subjected to residual stresses that emerge due to variations in the coefficient of thermal expansion or an atomic lattice spacing mismatch between the materials [36]. Several techniques that determine the residual stress state in thin films have been recently proposed: X-ray diffraction analysis [37–39], focused ion beam milling in combination with digital image correlation [40–43] and the Ion beam Layer Removal (ILR) method [44]. Experimental and computational results have shown that residual stresses can strongly influence the fracture behavior of materials [45–50]. Therefore, it is important to understand the influence of residual stresses on the crack driving force in multi-layered structures.

In this work, we investigate the influence of material inhomogeneities on the crack driving force in thin film stacks with an alternating arrangement of copper (Cu) and tungsten (W) layers deposited on a silicon (Si) wafer. It will be shown that the precise knowledge of the local material behavior as well as the magnitude and the distribution of residual stresses in a stack are important to appropriately calculate the crack driving force.

2. Evaluation of the crack driving force

2.1. Configurational forces and the J-integral

The configurational force concept is based on the ideas of Eshelby [51] and was expanded by Gurtin [52] and Maugin [53]. Configurational forces (CFs) describe the behavior of defects in materials without making any assumptions about the constitutive behavior of the materials. From a thermodynamics point of view, a CF tries to push a defect into a configuration where the total potential energy of the system has its minimum. In general, a CF vector $\mathbf{f}$ can be determined at each point in a body as

$$\mathbf{f} = -\nabla\cdot(\phi\mathbf{I} - \mathbf{F}^{\mathrm{T}}\mathbf{S}) \tag{1}$$

which is the divergence of the expression in parentheses, the so-called configurational stress tensor. In Eq. (1), ϕ is the strain energy density and $\mathbf{I}$ denotes the unity tensor. $\mathbf{F}^{\mathrm{T}}$ and $\mathbf{S}$ represent the transposed deformation gradient and 1st Piola-Kirchhoff stress tensor, respectively. The CF vector becomes non-zero only at positions of a defect in the body [18,54].

If we consider a two-dimensional homogeneous elastic body with a sharp crack, a CF vector $\mathbf{f}_{\mathrm{tip}}$ emerges at the crack tip. The projection of $\mathbf{f}_{\mathrm{tip}}$ in the crack extension direction gives the crack driving force

$$J_{\mathrm{tip}} = -\mathbf{e}\cdot\mathbf{f}_{\mathrm{tip}} \tag{2}$$

where $\mathbf{e}$ is the unit vector in crack propagation direction. If the body is externally loaded the crack driving force is equal to $J_{\mathrm{tip}} = J_{\mathrm{far}}$, where J_{far} is the far-field J-integral, which can be understood as the driving force induced by the external load in the body.

For simple cases, such as monotonic loading conditions and/or homogeneous materials, the J-integral calculated with the CF concept is equivalent to the conventional J-integral proposed by Rice in 1968 [55]. The conventional J-integral has been used as a loading parameter for cracks in the regime of elastic-plastic fracture mechanics. However, it has its limitations when applied for cases where non-proportional loading conditions prevail and, especially, for inhomogeneous materials, as pointed out in [18,54,56]. For the latter case where the J-integral becomes path dependent, the CF concept is very suitable for the determination of the crack driving force. This is described in the following section.

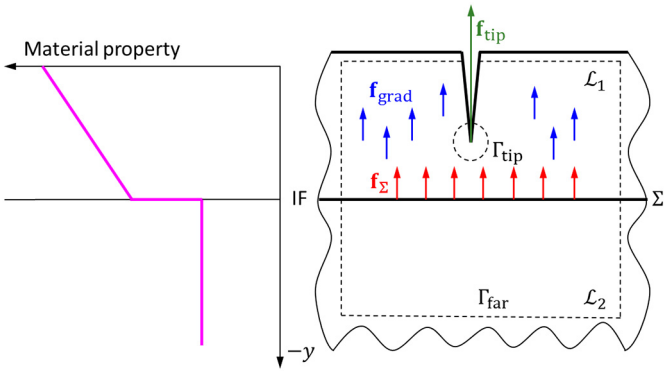

Fig. 1. Schematic distribution of configurational forces (CFs) in a two-layer component. The variation of material property, e.g. Young's modulus E, is shown on the left. CFs $\mathbf{f}_{\Sigma}$ are induced at the interface Σ due to the jump of E. CFs $\mathbf{f}_{\mathrm{grad}}$ are generated in layer $\mathscr{L}_1$ caused by the smooth E-variation. No CFs are present inside layer $\mathscr{L}_2$, since E = const. A single CF $\mathbf{f}_{\mathrm{tip}}$ emerges from the crack tip.

2.2. Evaluation of the material inhomogeneity effects

In a specimen where two material layers, $\mathscr{L}_1$ and $\mathscr{L}_2$, are separated by a sharp IF Σ, as sketched in Fig. 1 the material properties, e.g. the Young's modulus E, exhibit a jump at the IF, as depicted on the left side of Fig. 1. Due to this jump CFs are generated at the IF, given by the relation [19].

$$\mathbf{f}_{\Sigma} = -(\llbracket\phi\rrbracket\,\mathbf{I} - \llbracket\mathbf{F}^{\mathrm{T}}\rrbracket\langle\mathbf{S}\rangle)\mathbf{n} \tag{3}$$

In Eq. (3), $\llbracket q\rrbracket = (q^{+} - q^{-})$ denotes a jump of a quantity at the IF and $\mathbf{n}$ is the unit normal vector to the IF. $\langle q\rangle = (q^{+} + q^{-})/2$ represents the average of q across the interface.

Additionally, a smooth material property variation can be present *inside* of a layer, e.g. in layer $\mathscr{L}_1$. This gradient results in the formation of bulk CFs, given by [19].

$$\mathbf{f}_{\mathrm{grad}} = -\nabla_{\mathbf{x}}\phi(\mathbf{F},\mathbf{x}) \tag{4}$$

The strain energy density ϕ in Eq. (4) depends on the reference coordinate $\mathbf{x} = \mathbf{x}(x,y,z)$ and $\nabla_{\mathbf{x}}$ denotes the explicit gradient in the reference frame. For the example of a gradient in Young's modulus E in y-direction as shown in Fig. 1, $\mathbf{f}_{\mathrm{grad}}$ has only a y-component given by $f_{\mathrm{grad},y} = \frac{\partial\phi}{\partial E}\frac{\partial E}{\partial y}$.

The CF vector emerging at the crack tip $\mathbf{f}_{\mathrm{tip}}$ and, therefore, the magnitude of the crack driving force, see Eq. (2), are strongly affected by the CFs induced at the IF and in the bulk. This effect is quantified by two terms [19]:

An *interface inhomogeneity term* C^{IF}, corresponding to the sum of all CFs $\mathbf{f}_{\Sigma}$ that are generated at the sharp IF Σ

$$C^{\mathrm{IF}} = -\mathbf{e}\cdot\int_{\Sigma}\mathbf{f}_{\Sigma}\,dl \tag{5}$$

A *gradient term* C^{GRAD}, corresponding to the sum of all CFs $\mathbf{f}_{\mathrm{grad}}$ inside of a material layer $\mathscr{L}$

$$C^{\mathrm{GRAD}} = -\mathbf{e}\cdot\int_{\mathscr{L}}\mathbf{f}_{\mathrm{grad}}\,dA \tag{6}$$

The sum of all inhomogeneity effects in the body,

$$C_{\mathrm{inh}} = C^{\mathrm{IF}} + C^{\mathrm{GRAD}} \tag{7}$$

represents the so-called *material inhomogeneity term*. In order to satisfy the equilibrium of CFs [52,53], the crack driving force in inhomogeneous materials is given by the following relation, see e.g. [18,19]:

$$J_{tip} = J_{far} + C_{inh} \tag{8}$$

where J_{far} is calculated around the far-field contour Γ_{far}, as shown in Fig. 1. The material inhomogeneity term C_{inh} can be understood as the crack driving force term that is induced at a given loading J_{far} in the specimen due to the material inhomogeneity. An anti-shielding effect is described by a positive and shielding by a negative value of C_{inh}.

A material inhomogeneity effect is also induced, if the material properties are constant, but thermal strains or eigenstrains (or the resulting eigenstresses) exhibit jumps or smooth variations [19,35]. Eqs. (3)–(8) can be applied for the evaluation of the CFs due to a jump of the eigenstrain at an IF or smooth eigenstrain gradients and the resulting effects on the crack driving force.

If a component consists of i layers with smooth material or eigenstrain gradients, the gradient term is given by the summation $C^{GRAD} = \Sigma_i C_i^{GRAD}$. Likewise, if there are j interfaces present in the component where the material properties or eigenstrains have a jump, the interface inhomogeneity term is given by $C^{IF} = \Sigma_j C_j^{IF}$.

If both, the material properties and eigenstrains inside of the layers are constant, as in layer $\mathscr{L}_2$ in Fig. 1, C^{GRAD} is zero. This was the case in a previous study of a macroscopic ceramic multilayer composite where only the interface inhomogeneity term C^{IF} had to be considered [57]. In our current investigation, the gradient inhomogeneity term C^{GRAD} must be taken into account, since the variation of residual stresses inside the layers leads to an explicit gradient of the strain energy density.

3. Thin film stack characterization

3.1. Material characteristics

The thin films in the current investigation were prepared by physical vapor deposition. Depending on the film sequence, W and Cu films were stacked on top of each other in subsequent steps to form W-Cu-W and Cu-W-Cu stacks on Si wafers without disrupting the vacuum in the deposition chamber. Each layer has an approximate thickness of 500 nm. W and Cu have a nanocrystalline structure with a globular grain size varying between 60 and 70 nm, determined by a line intercept method from scanning electron microscopy (SEM) images [58].

The difference of the elastic-plastic properties between the W and Cu films mainly determines the material inhomogeneity effect at the IFs. While W is a very stiff and strong material, Cu is ductile and has a higher fracture toughness. The Si substrate in our investigations is assumed to behave linear elastically. The elastic properties of Si, W and Cu are taken from literature, as summarized in [58,59]. To determine the flow behavior of the thin W and Cu films, a new approach was proposed in our previous investigation [13]. In brief, the yield stress σ_y and the hardening parameter n are optimized to fit the force-displacement response from simulations to an experimental spherical nanoindentation curve. The elastic and plastic material data of Si, W and Cu in the thin film stack are given in Table 1.

In addition to the material property variations between the different layers, a spatial variation of residual stresses exists in the stacks. These residual stresses vary not only at the IFs between the layers, but also inside the W and Cu films. In a previous analysis [58], we have determined the residual stress variation in the W-Cu-W and Cu-W-Cu stacks with the Ion beam Layer Removal (ILR) method [44]. Details about these experiments and the analysis can be found in [58]. The residual stress variations for the W-Cu-W and the Cu-W-Cu material systems in relation to the cutting depth are shown in Fig. 2. The residual stresses have an average value of about 0.25 GPa in the Cu-layers of both stack configurations. The W-layers exhibit compressive residual stresses and especially the W-layer on top of the Si substrate in the W-Cu-W stack has a strong gradient and a peak residual stress of about −1.25 GPa.

Table 1
Material properties for the Si-, W- and Cu-layers in the thin film stack: Young's modulus E, Poisson's ratio ν, yield strength σ_y, and hardening parameter n. The latter two values were determined for W and Cu in [13]. Si behaves linear elastically in every model.

Material	E [GPa]	ν	σ_y [GPa]	n
Si	170	0.28	–	–
W	411	0.28	1.91	13.3
Cu	130	0.34	0.65	2.8

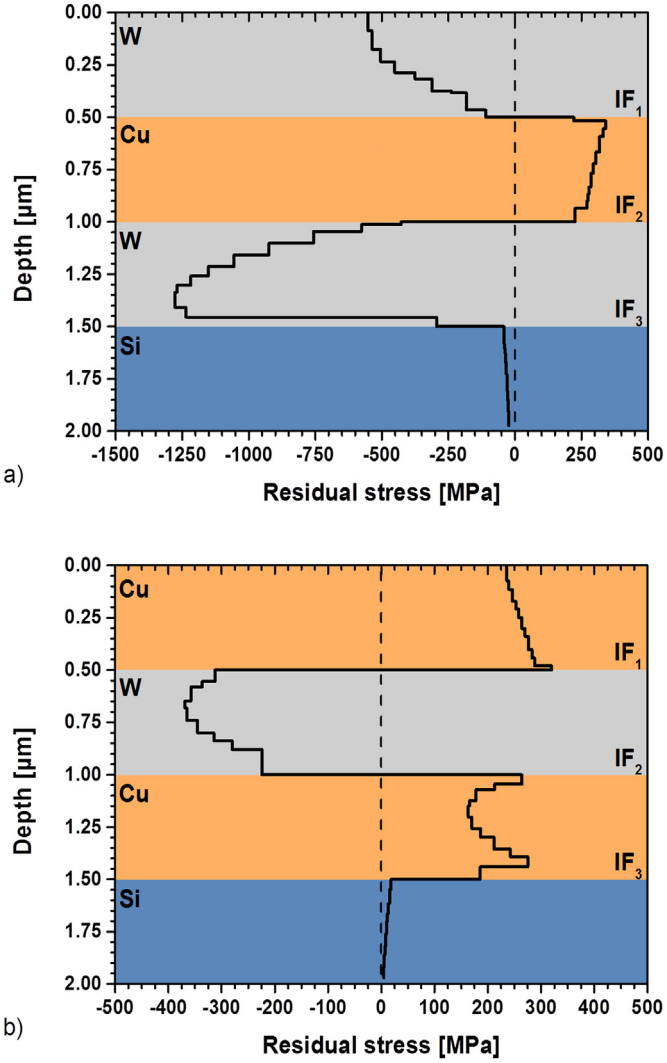

Fig. 2. Residual stress distribution for a) the W-Cu-W stack, b) the Cu-W-Cu stack.

3.2. Fracture simulations

Finite element (FE) simulations are conducted to determine the material inhomogeneity effect and the crack driving force J_{tip} in the W-Cu-W and Cu-W-Cu stacks. The simulations are performed with the commercial FE software package ABAQUS (Simulia, Dassault Systems). The models are based on the geometries of micro-beams which were prepared for the fracture experiments in a previous study [60], as shown in the SEM image in Fig. 3a. The exact geometries for the W-Cu-W and Cu-W-Cu specimens are given in Table 2.

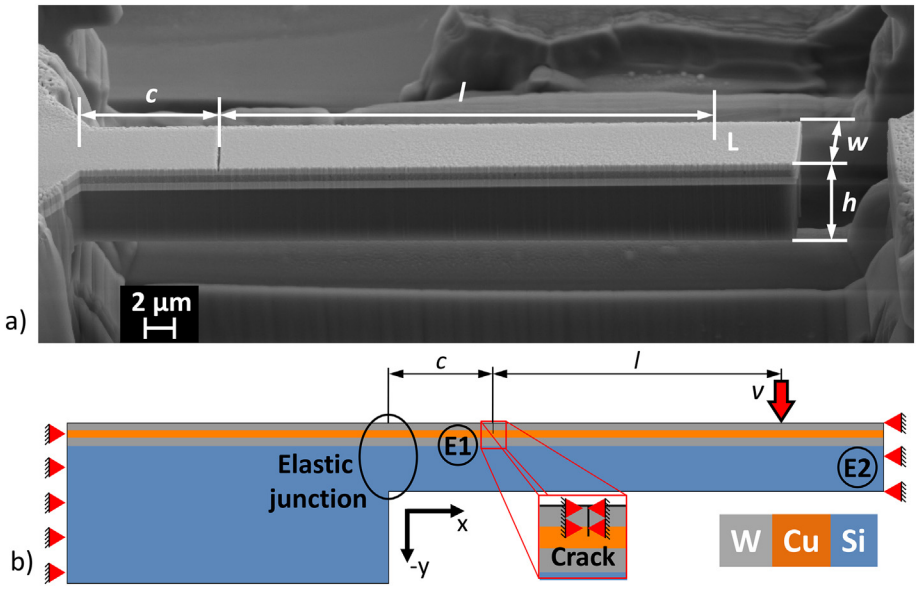

Fig. 3. a) SEM micrograph of the W-Cu-W micro-cantilever beam with indicated geometry, the distance c between the crack and beam fixation, the spacing l between the loading point L and the crack, the total beam height h, and width w. The thickness of each layer is measured from SEM micrographs at higher magnification. b) 2D FE model of the micro-cantilever beam in its initial state. In this constellation the beam front and crack flanks are restricted from movement before the residual stresses are equilibrated. The elastic junction, equilibration steps E1 and E2 as well as the loading position L are indicated in the schematic.

Table 2
Micro cantilever beam dimensions determined from experiments.

Stack	c [µm]	l [µm]	h [µm]	w [µm]
W-Cu-W-Si	6.79	20.50	4.50	3.76
Cu-W-Cu-Si	3.80	21.90	4.50	4.10

A linear elastic (LE) model and an elastic-plastic model with residual stresses (EP-RS) are used for the calculations. The LE model only considers the linear elastic material properties from Table 1 and does not account for the residual stresses of Fig. 2. The EP-RS model incorporates the flow behavior from Table 1 and the residual stress variations. The 2D plane strain model is shown in Fig. 3b. In order to determine the variation of the crack driving force for a crack propagating through the material stack, models are generated for crack lengths between 0.1 and 1.475 µm.

Each model is meshed with four-node bilinear plane strain elements (CPE4). An area around the crack tip, covering the thickness of the layer in y-direction and double the thickness in x-direction, is meshed with square-shaped elements with a constant size of 0.005 µm. By using this element size we are able to accurately model cracks which are a distance of 0.025 µm apart from the closest IF. A free mesh has been put on the remaining area with the constraint that the largest elements do not exceed a size of 0.3 µm. In order to properly calculate the material inhomogeneity term at the material boundaries, also the mesh around the sharp IFs is resolved with the smallest elements.

The modeling steps for the EP-RS model are the following:

1. Insertion of residual stresses.
2. Insertion of a crack.
3. First equilibration of residual stresses, denoted by E1 in Fig. 3b.
4. Release of beam front and equilibration of residual stresses, denoted by E2 in Fig. 3b.
5. Mechanical loading.

To perform the simulation for the simpler LE model only steps 2 and 5 need to be considered from the above list.

In the EP-RS model the residual stresses from Fig. 2 are imposed on the element integration points via the user subroutine SIGINI during step 1. The crack lies perpendicular to the IFs and $(0, -1)$ is designated to be the crack propagation direction. In order to introduce a crack, a so-called "seam" is defined in the model, i.e. a line along which the nodes are duplicated. Initially, the flank nodes are fixed in all directions, as shown in the insert of Fig. 3b. After that the residual stresses are equilibrated in step 3 by releasing the crack flank nodes, denoted by equilibration step E1 in Fig. 3b. Subsequently, the front of the beam is released in step 4, redistributing the residual stresses once again. This procedure is able to reproduce the residual stress redistribution due to the insertion of a thin notch into the sample and the subsequent release of the right end of the beam (E2) by focused ion beam milling [60].

While the micro-beam is loaded, the left side of the beam remains constrained in all directions. By choosing this kind of boundary condition, the simulated force-displacement behavior shows a good agreement with the mechanical response of the micro-beam in the experiment, as presented in [60]. The micro-beam is monotonically loaded by displacing it by $v = 1.5$ µm at the loading point L, as shown in Fig. 3b.

The CFs determining the crack driving force J_{tip} in the system are calculated with a post-processing routine following the conventional FE analysis. Details about the numerical calculation of CFs can be found in [61,62]. Our post-processing tool collects the displacement, stress and strain energy density fields from the FE simulations and calculates the CF for each node in the model. The crack driving force J_{tip} is determined with Eq. (8) by summing up the contributions calculated with Eqs. (5) and (6) as well as the far-field J-integral J_{far}.

Note that the residual stresses in the film stacks are not a consequence of a mismatch of the thermal expansion coefficient, as the thin films were deposited at room temperature. This is why the residual stress state is introduced in the model as an initial condition via SIGINI. The implementation routine was verified by calculating the far-field J-integral J_{far} with the CF post-processing tool as well as the virtual crack extension (VCE) method provided by ABAQUS. It was confirmed that both approaches yield the same result for J_{far}.

4. Results and discussion

4.1. Material inhomogeneity effects

The material inhomogeneity term C_{inh}, the interface inhomogeneity term C^{IF} and gradient term C^{GRAD} are calculated for stationary cracks with increasing crack length by utilizing Eqs. (5)–(7). The different material inhomogeneity terms for the W-Cu-W and Cu-W-Cu stacks versus the crack length are plotted in Figs. 4 and 5, respectively.

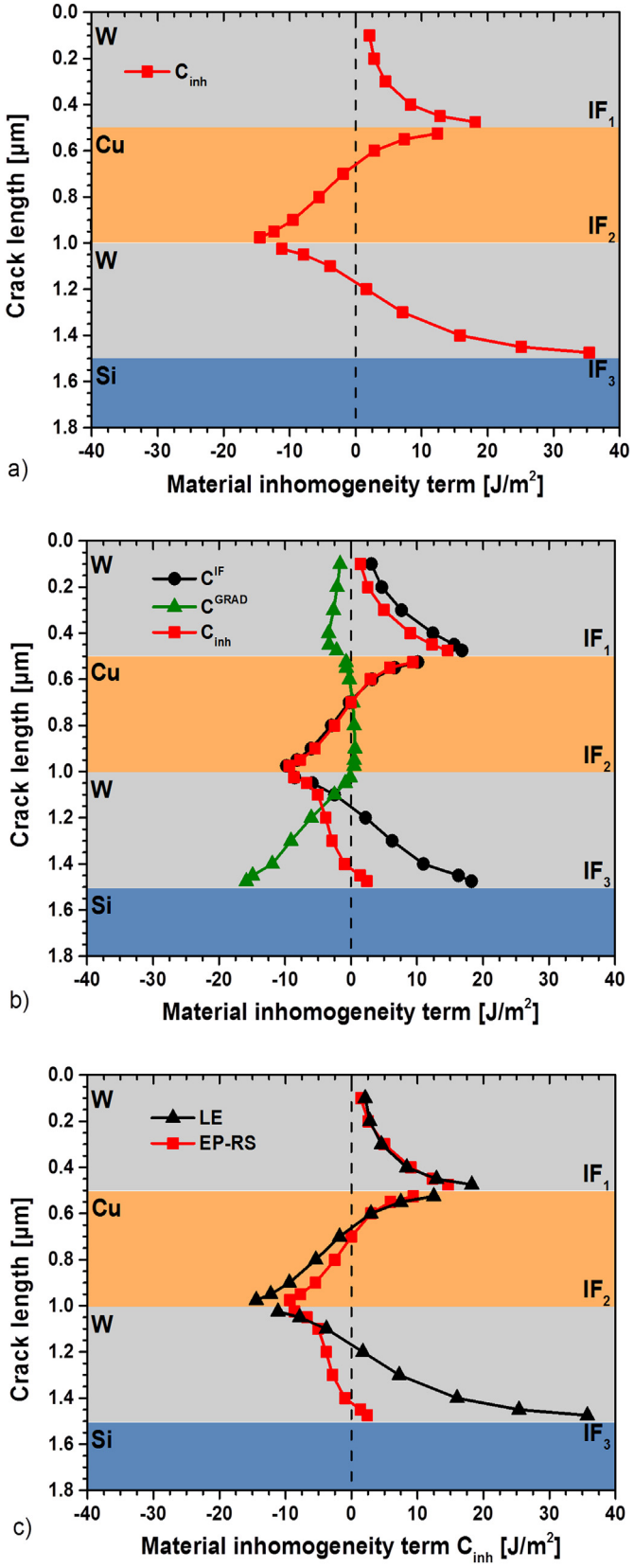

Fig. 4. The material inhomogeneity effect in the W-Cu-W specimen for a load point displacement of $v = 1.5$ µm. a) Material inhomogeneity term C_{inh} for the LE model (without residual stresses). b) Interface inhomogeneity term C^{IF}, gradient term C^{GRAD} and the material inhomogeneity term C_{inh} for the EP-RS model (with the residual stress distribution from Fig. 2a). c) Comparison between the material inhomogeneity terms C_{inh} from the LE and the EP-RS models.

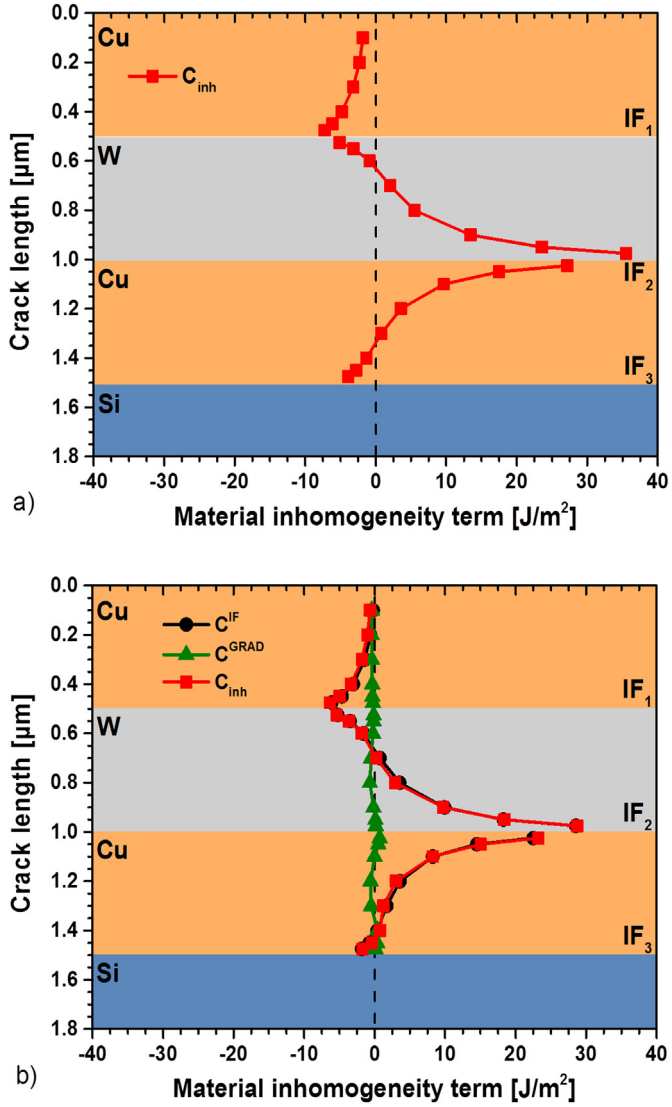

Fig. 5. The material inhomogeneity effect in the Cu-W-Cu specimen for a load point displacement $v = 1.5$ µm. a) Material inhomogeneity term C_{inh} for the LE model (without residual stresses). b) Interface inhomogeneity term C^{IF}, gradient term C^{GRAD} and the material inhomogeneity term C_{inh} for the EP-RS model (with the residual stress distribution from Fig. 2b).

4.1.1. W-Cu-W stack

Fig. 4a shows the material inhomogeneity term C_{inh} for the LE model of the W-Cu-W stack. As mentioned before the residual stresses are neglected in this model. Thus, the total material inhomogeneity term C_{inh} coincides with the interface inhomogeneity term C^{IF}. W has a larger Young's modulus E than Cu and Si. Therefore, a crack approaching the W/Cu- or W/Si-IF experiences an increasing anti-shielding effect. However, as the crack extends through the Cu film, the Cu/W-IF is starting to shield the crack tip. Shielding starts after the crack reaches approximately a length of 0.7 µm and C^{IF} becomes negative. The maximum and minimum values of C^{IF}, which lie exactly at the IFs, are numerically not accessible in the FE modeling.

In Fig. 4b the inhomogeneity terms are plotted for the EP-RS model, which takes into account the residual stress distribution from Fig. 2a. The gradient term C^{GRAD} (green line with triangles), the interface inhomogeneity term C^{IF} (black line with circles), and the material inhomogeneity term C_{inh} (red line with squares), are plotted as a function of the crack length. Maximum anti-shielding occurs at IF_1, whereas IF_2 provides the highest shielding effect. At the third IF, the shielding effect from the residual stress gradient and the anti-shielding effect caused by

the jump of material properties at IF_3 nearly compensate. The gradient term is small in the first W-layer and negligible in the Cu-interlayer.

The influence of the residual stress distribution, and especially the gradient term C^{GRAD}, becomes evident by comparing the C_{inh} curves in Fig. 4a and b, see Fig. 4c. The largest difference appears at IF_3. As the crack tip is noticeably shielded by the negative compressive residual stress gradient in the bottom W-layer in the EP-RS model, most of the anti-shielding present in the LE model is annihilated or even reverted into a slight shielding effect. This will have implications when calculating the crack driving force, see Section 4.2.

4.1.2. Cu-W-Cu stack

Fig. 5a shows the material inhomogeneity term C_{inh} for the LE model of the Cu-W-Cu stack. The Cu/W- and Cu/Si-IFs provide small shielding effects, whereas the W/Cu-IF shows a large anti-shielding effect to the crack tip.

The material inhomogeneity terms for the EP-RS model are given in Fig. 5b. The gradient term C^{GRAD} is vanishingly small as the residual stress gradients are low and has hardly any influence on the material inhomogeneity term. C_{inh} is almost identical to the interface inhomogeneity term C^{IF}. Only small differences occur between the C_{inh} curves of the LE model and the EP-RS model.

4.2. Crack driving force and fracture toughness determination

The crack driving force J_{tip} is plotted against the crack length for the W-Cu-W and the Cu-W-Cu models in Fig. 6a and b, respectively. In both figures, the LE model and the EP-RS model are compared. The thin vertical line denotes the fracture toughness of the W-layer measured in terms of the critical J-integral J_C. Note that a crack can propagate if the crack driving force equals or exceeds this critical value, i.e. if $J_{tip} \geq J_C$.

For homogeneous materials under bending the fracture toughness, measured in terms of the critical stress intensity factor K_C, can easily be determined experimentally from the fracture stress σ_F, the initial crack length and the geometry of the specimen, see e.g. [60,63]. K_C is a valid parameter, if the conditions of linear fracture mechanics (LEFM) are fulfilled [64]. In thin film stacks containing soft metals, such as Cu, LEFM will not often be applicable. Elastic−plastic fracture mechanics should be applied instead, where the critical J-integral J_C characterizes the fracture toughness. For LEFM and plane strain conditions the parameters J_C and K_C are connected by the relation [64],

$$J_C = K_C^2(1 - \nu^2)/E \tag{9}$$

where E is the Young's modulus and ν the Poisson's ratio.

In order to determine the intrinsic fracture toughness J_C for materials in thin film systems, experiments and numerical modeling must be combined. In the experiment the critical load F_C (or critical displacement v_C) is determined where crack propagation starts. The crack driving force at this critical load,

$$J_{tip}(F_C) = J_C \tag{10}$$

is determined by the FE modeling with CF-post processing.

As an example, we have simulated the force−displacement response of a notched W-Cu-W specimen with the geometries from Table 2 by using the EP-RS model, as introduced in Section 3.2. For an initial crack length $a_0 = 0.44$ µm, crack growth in the top W-layer started in an unstable manner at a critical displacement of $v_C = 1.3$ µm, which corresponds to a critical load $F_C = 0.65$ mN. From the performed simulation we have evaluated the values of J_{far}, C_{inh} and J_{tip} for these critical conditions. The resulting critical J-integral value is $J_C = 21.2$ J/m^2; this corresponds with Eq. (9) to $K_C = 3.07$ MPa$\sqrt{\text{m}}$. In a previous study [60], the critical J-integral was determined without taking into account the gradient of the residual stresses C^{GRAD}. The result was $J_C = 25.2$ J/m^2 ($K_C = 3.35$ MPa$\sqrt{\text{m}}$), i.e. the previous estimate of J_C was 19% too high. It should be mentioned that a complete negligence of the material inhomogeneity effect, i.e. the assumption of a homogeneous cantilever material, would result a value of $J_C = 2.8$ J/m^2 ($K_C = 1.12$ MPa$\sqrt{\text{m}}$) [60].

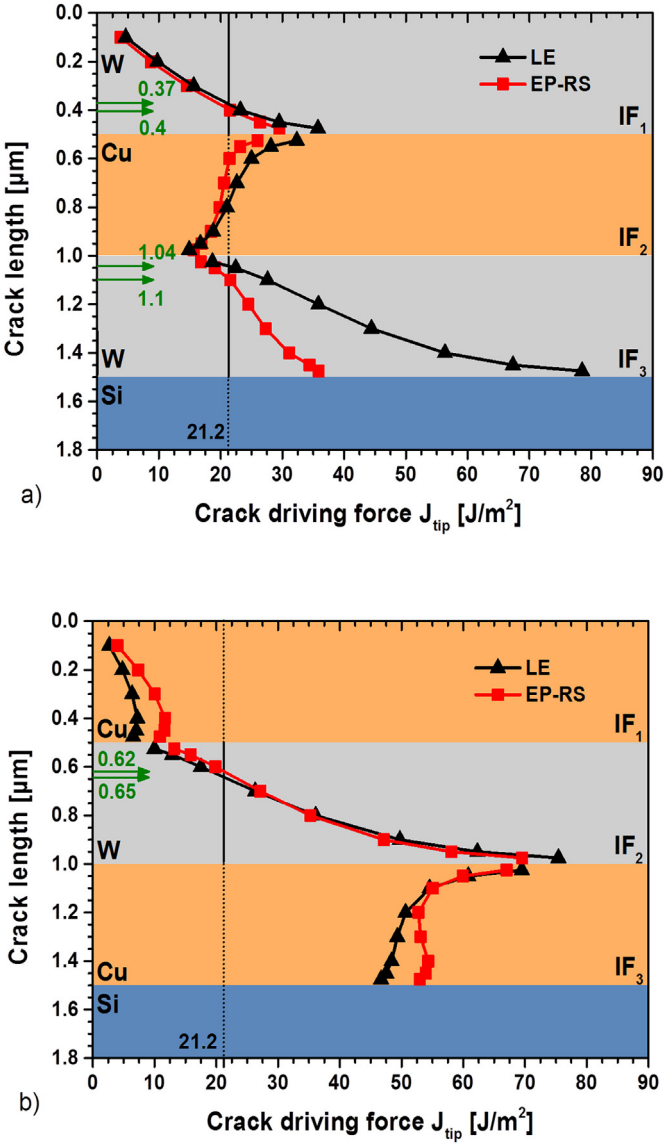

Fig. 6. a) Variation of the crack driving force J_{tip} in the W-Cu-W stack for a load point displacement $v = 1.5$ µm. The critical crack tip positions for the LE and EP-RS model in the W-layers are highlighted by green arrows. b) Variation of the crack driving force J_{tip} in the W-Cu-W stack for a load point displacement $v = 1.5$ µm. The critical crack tip positions for the LE and EP-RS model in the W-layers are highlighted by green arrows. (For interpretation of the references to colour in this figure legend, the reader is referred to the web version of this article.)

The difference of 19% between the previous and current numerical results strongly suggests that the gradient term C^{GRAD}, resulting from the residual stress gradients, has to be considered when calculating the crack driving force. Otherwise, fallacious predictions about the critical loading conditions of components with similar structures cannot be excluded. Such critical loading conditions are discussed below.

4.3. Critical loading conditions of the thin film stack

We can assume that all W-layers in our stacks have the same intrinsic fracture toughness, $J_C = 21.2$ J/m^2, independent of the crack tip position, see the vertical lines in Fig. 6a and b. From Fig. 6a we can see that a crack in the top W-layer of the W-Cu-W stack starts to propagate

at a load point displacement, $v = 1.5$ μm, if the crack length exceeds $a_c = 0.40$ μm for the EP-RS model ($a_c = 0.37$ μm for the LE model), as marked by the green arrows.

Since J_{tip} increases with increasing crack length, the crack propagates unstably to the W/Cu-IF. The fracture toughness for the nanocrystalline Cu-film is not known, but it can be assumed that J_C is considerably higher than for the W-film, since Cu has a lower yield strength and behaves more ductile than W. Even if this were not so, the crack would stop inside the Cu-layer due to the strong shielding effect from the Cu/W-IF, see Fig. 4. Thus, the soft Cu-interlayer in the W-Cu-W stack offers an arresting environment for a crack propagating from the surface of the cantilever beam. After the top W-layer fails and the crack enters the Cu-interlayer the crack driving force decreases with crack length due to the repelling effect of the Cu/W-IF, as shown in Fig. 6a. In order to achieve further crack propagation, the external load on the micro-beam has to be strongly increased. The arresting ability of soft interlayers has also been demonstrated in other investigations, see e.g. [23,65].

For a crack in the second W-layer that has penetrated the Cu-layer, the critical crack length is 1.10 μm for the EP-RS model ($a_c = 1.04$ μm for the LE model). In this layer, the J_{tip}-curves of the two models strongly differ. The comparison of the C_{inh} curves in Fig. 4c reveals that here the gradient term due to the high compressive residual stress gradient plays an important role. Due to the increase of J_{tip} the crack grows in an unstable manner towards the W/Si-interface, IF_3. The remaining structure consists of only the Si wafer. As reported in [66], the fracture toughness of single-crystalline Si ranges between $K_C = 0.7$ and 2.1 MPa$\sqrt{m}$, corresponding to $J_C = 1.1$ and 9.9 J/m^2. A comparison of the upper limit of the fracture toughness with the crack driving force for a crack tip in Si at IF_3, $J_{tip} \approx 35$ J/m^2, shows that catastrophic fracture of the remaining Si-layer will occur.

The crack driving force J_{tip} in the Cu-W-Cu stack, see Fig. 6b, is given by the sum of the far-field J-integral J_{far} and the interface inhomogeneity term C^{IF}, as C^{GRAD} is almost zero. A comparison of the curves for the crack tip located in the first Cu-layer shows that the J_{tip} values for the EP-RS model are almost twice as high as for the LE model. The difference will further increase with higher loading. This shows that the consideration of the elastic-plastic behavior and the physically correct application of nonlinear fracture mechanics can be decisive for the correct prediction of multi-layer stacks with ductile film materials.

A crack which has penetrated the first Cu layer reaches its critical length at $a_c = 0.62$ μm for the EP-RS model ($a_c = 0.65$ μm for the LE model). Since the crack driving force strongly increases with increasing crack length, the crack will grow immediately through the whole W-layer. Although the crack driving force decreases after the crack has entered the Cu-layer, it remains relatively high at a value of $J_{tip} \approx 53$ J/m^2. Since we do not know the J_C value for the thin Cu film, we cannot predict whether the conditions in the second Cu-layer are critical or not. In the experiments, fracture in the Cu-layers was not observed, indicating that the J_C value for Cu should be a lot higher than the one for W.

4.4. Validity check of fracture mechanics parameters

The applicability of linear elastic or elastic-plastic fracture mechanics in thin film stacks with such small thickness dimensions might be questioned by some readers. In order to check the validity of the fracture mechanics parameters, we have considered two possible crack tip positions in the W-Cu-W thin film stack and plotted the stresses normal to the crack plane σ_{xx} against the distance from the crack tip r in a log-log scale, as shown in Fig. 7a and b. A similar check has been presented, e.g. in [64].

The stress and strain field in front of the crack tip can be characterized by the stress intensity factor K if the conditions of LEFM prevail and the stresses are proportional to $1/\sqrt{r}$ [64]. In a similar manner the J-integral characterizes the crack tip field in the regime of

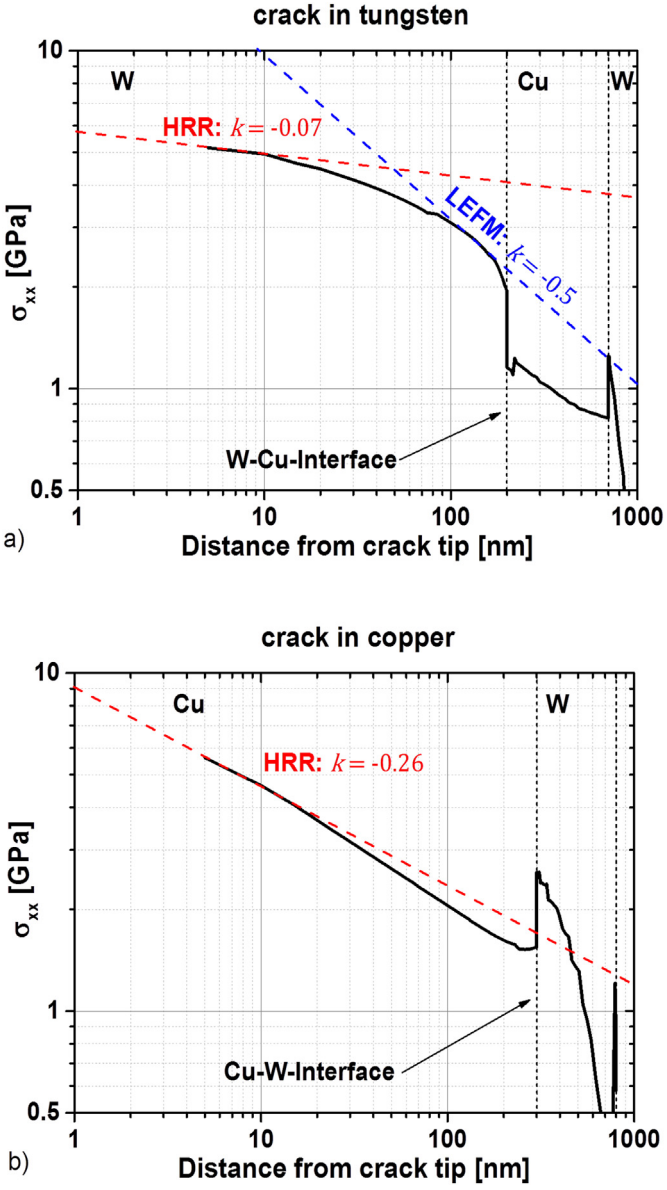

Fig. 7. Log-log plots for two different crack tip positions in the W-Cu-W stack to check the validity of fracture mechanics parameters K and J. a) Crack tip located in the top W-layer, crack length $a = 0.3$ μm. b) Crack tip located in the Cu-interlayer, crack length $a = 0.7$ μm.

elastic-plastic fracture mechanics, if the stresses vary as $r^{-1/(1+n)}$, given by the so-called HRR-solution [64].

Fig. 7a shows the behavior around a crack tip positioned in the top W-layer, for a crack length $a = 0.3$ μm and a point load displacement of $v = 1.5$ μm. It is seen that the stresses very close to the crack tip follow the HRR-solution. In the log-log plot, this behavior is given by a linear curve with the slope $k = -\frac{1}{1+n} = -0.07$, for $n = 13.3$ for W from Table 1. Additionally, a K-dominated zone might exist between $r \approx 100$ and 180 nm exhibiting a slope of $k = -\frac{1}{2}$; however, this is somewhat uncertain. In this case both K and J would characterize the crack tip conditions at this load. It should be noted that the magnitudes of the K- and J-dominated regions decrease with increasing load [64].

In the case of a crack in the Cu-layer with crack length $a = 0.7$ μm and a point load displacement of $v = 1.5$ μm, a K-dominated zone does not exist in front of the crack tip, see Fig. 7b. However, a J-dominated zone is visible near the crack tip with a slope of $k = -0.26$ for $n = 2.8$ from Table 1.

Concluding this section, we can state that J is a valid fracture

mechanics parameter in such thin film stacks and that the determined critical J-integral value of $J_C = 21.2$ J/m^2 for the W-films is physically appropriate. This is so as long as the assumption of a homogeneous material behavior within each layer is appropriate. A final remark shall be made: J-dominance does not necessarily imply agreement with the HRR crack tip field solution. This means, J can be a useful fracture mechanics parameter even in cases where the log-log plot of Fig. 7a would show no region with a slope $= -\frac{1}{1+n}$, see [64] for details.

5. Summary

The crack arresting capabilities of two thin film systems have been investigated exemplarily for a W-Cu-W and a Cu-W-Cu stack configuration.

It was demonstrated that the intrinsic fracture toughness of single material layers in complex thin film stacks can be determined in terms of the critical J-integral J_C by combining experimental results and finite element modeling utilizing the concept of configurational forces. It was shown that also the residual stress gradients must be considered to accurately determine J_C.

The application of the concept of configurational forces is a convenient tool for calculating the crack driving force in structures with complex design and material property and residual stress variations. The concept is not limited by the dimensions of the investigated components. It can be very useful for the design of tough and damage tolerant thin film stacks.

Smart design of thin films in form of alternate layers with different material properties can significantly increase the fracture toughness of a component. We have shown that in a W-Cu-W film stack the crack arrests in the soft Cu-interlayer so that the load necessary for further crack propagation has to be significantly increased.

In a similar way, spatial variations of residual stresses can be utilized. High compressive residual stresses and residual stress gradients can dramatically increase the critical defect size which the structure is able to contain at a given load.

Acknowledgements

Financial support by the Austrian Federal Government (in particular from Bundesministerium für Verkehr, Innovation und Technologie and Bundesministerium für Wissenschaft, Forschung und Wirtschaft) represented by Österreichische Forschungsförderungsgesellschaft mbH and the Styrian and the Tyrolean Provincial Government, represented by Steirische Wirtschaftsförderungsgesellschaft mbH and Standortagentur Tirol, within the framework of the COMET Funding Programme (Projects A7.17 and A1.3) is gratefully acknowledged.

References

[1] E.O. Hall, The deformation and ageing of mild steel III Discussion of results, Proc. Phys. Soc. Sect. B 64 (1951) 747, https://doi.org/10.1088/0370-1301/64/9/303.
[2] N.J. Petch, The cleavage strength of polycrystals, J. Iron Steel Inst. 174 (1953) 25–28, https://doi.org/10.1007/BF01972547.
[3] M.A. Meyers, A. Mishra, D.J. Benson, Mechanical properties of nanocrystalline materials, Prog. Mater. Sci. 51 (2006) 427–556, https://doi.org/10.1016/j.pmatsci.2005.08.003.
[4] H. Conrad, Grain size dependence of the plastic deformation kinetics in Cu, Mater. Sci. Eng. A 341 (2003) 216–228, https://doi.org/10.1016/S0921-5093(02)00238-1.
[5] M.D. Uchic, D.M. Dimiduk, J.N. Florando, W.D. Nix, Sample dimensions influence strength and crystal plasticity, Science 305 (2004) 986–989, https://doi.org/10.1126/science.1098993.
[6] J.R. Greer, W.C. Oliver, W.D. Nix, Size dependence of mechanical properties of gold at the micron scale in the absence of strain gradients, Acta Mater. 53 (2005) 1821–1830, https://doi.org/10.1016/j.actamat.2004.12.031.
[7] S.P. Baker, Plastic deformation and strength of materials in small dimensions, Mater. Sci. Eng. A 319–321 (2001) 16–23, https://doi.org/10.1016/S0921-5093(00)02004-9.
[8] W.D. Nix, Mechanical properties of thin films, Metall. Trans. A. 20 (1989) 2217–2245, https://doi.org/10.1007/BF02666659.
[9] J.Y. Kim, D. Jang, J.R. Greer, Tensile and compressive behavior of tungsten, molybdenum, tantalum and niobium at the nanoscale, Acta Mater. 58 (2010) 2355–2363, https://doi.org/10.1016/j.actamat.2009.12.022.
[10] D. Kiener, C. Motz, W. Grosinger, D. Weygand, R. Pippan, Cyclic response of copper single crystal micro-beams, Scr. Mater. 63 (2010) 500–503, https://doi.org/10.1016/j.scriptamat.2010.05.014.
[11] D. Kiener, W. Grosinger, G. Dehm, R. Pippan, A further step towards an understanding of size-dependent crystal plasticity: in situ tension experiments of miniaturized single-crystal copper samples, Acta Mater. 56 (2008) 580–592, https://doi.org/10.1016/j.actamat.2007.10.015.
[12] D. Jang, J.R. Greer, Size-induced weakening and grain boundary-assisted deformation in 60 nm grained Ni nanopillars, Scr. Mater. 64 (2011) 77–80, https://doi.org/10.1016/j.scriptamat.2010.09.010.
[13] D. Kozic, V. Maier-Kiener, R. Konetschnik, H.-P. Gänser, T. Antretter, R. Brunner, D. Kiener, Extracting flow curves from nano-sized metal layers in thin film systems, Scr. Mater. 130 (2017) 143–147, https://doi.org/10.1016/j.scriptamat.2016.11.008.
[14] A. Rinaldi, P. Peralta, C. Friesen, K. Sieradzki, Sample-size effects in the yield behavior of nanocrystalline nickel, Acta Mater. 56 (2008) 511–517, https://doi.org/10.1016/j.actamat.2007.09.044.
[15] R. Fritz, V. Maier-Kiener, D. Lutz, D. Kiener, Interplay between sample size and grain size: single crystalline vs. ultrafine-grained chromium micropillars, Mater. Sci. Eng. A 674 (2016) 626–633, https://doi.org/10.1016/j.msea.2016.08.015.
[16] A. Pineau, A. Amine Benzerga, T. Pardoen, Failure of metals III: fracture and fatigue of nanostructured metallic materials, Acta Mater. 107 (2016) 508–544, https://doi.org/10.1016/j.actamat.2015.07.049.
[17] O. Kolednik, L. Nicolais, Fracture mechanics, Wiley Encycl. Compos. John Wiley & Sons, Inc., 2011, , https://doi.org/10.1002/9781118097298.weoc096.
[18] N.K. Simha, F.D. Fischer, O. Kolednik, C.R. Chen, Inhomogeneity effects on the crack driving force in elastic and elastic-plastic materials, J. Mech. Phys. Solids 51 (2003) 209–240, https://doi.org/10.1016/S0022-5096(02)00025-X.
[19] N.K. Simha, F.D. Fischer, O. Kolednik, J. Predan, G.X. Shan, Crack tip shielding or anti-shielding due to smooth and discontinuous material inhomogeneities, Int. J. Fract. 135 (2005) 73–93, https://doi.org/10.1007/s10704-005-3944-5.
[20] Q.H. Qin, X. Zhang, Crack deflection at an interface between dissimilar piezoelectric materials, Int. J. Fract. 102 (2000) 355–370, https://doi.org/10.1023/A:1007601312977.
[21] L. Guo, T. Kitamura, Y. Yan, T. Sumigawa, K. Huang, Fracture mechanics investigation on crack propagation in the nano-multilayered materials, Int. J. Solids Struct. 64 (2015) 208–220, https://doi.org/10.1016/j.ijsolstr.2015.03.025.
[22] O. Kolednik, J. Predan, F.D. Fischer, P. Fratzl, Improvements of strength and fracture resistance by spatial material property variations, Acta Mater. 68 (2014) 279–294, https://doi.org/10.1016/j.actamat.2014.01.034.
[23] M. Sistaninia, O. Kolednik, Improving strength and toughness of materials by utilizing spatial variations of the yield stress, Acta Mater. 122 (2017) 207–219, https://doi.org/10.1016/j.actamat.2016.09.044.
[24] P. Fratzl, O. Kolednik, F.D. Fischer, M.N. Dean, The mechanics of tessellations – bioinspired strategies for fracture resistance, Chem. Soc. Rev. 45 (2015) 252–267, https://doi.org/10.1039/C5CS00598A.
[25] U.G.K. Wegst, H. Bai, E. Saiz, A.P. Tomsia, R.O. Ritchie, Bioinspired structural materials, Nat. Mater. 14 (2015) 23–36, https://doi.org/10.1038/nmat4089.
[26] O. Kolednik, J. Predan, F.D. Fischer, P. Fratzl, Bioinspired design criteria for damage-resistant materials with periodically varying microstructure, Adv. Funct. Mater. 21 (2011) 3634–3641, https://doi.org/10.1002/adfm.201100443.
[27] P. Fratzl, H.S. Gupta, F.D. Fischer, O. Kolednik, Hindered crack propagation in materials with periodically varying young's modulus - Lessons from biological materials, Adv. Mater. 19 (2007) 2657–2661, https://doi.org/10.1002/adma.200602394.
[28] S. Suresh, Y. Sugimura, T. Ogawa, Fatigue cracking in materials with brittle surface coatings, Scr. Metall. Mater. 29 (1993) 237–242, https://doi.org/10.1016/0956-716X(93)90315-J.
[29] R. Pippan, K. Flechsig, F.O. Riemelmoser, Fatigue crack propagation behavior in the vicinity of an interface between materials with different yield stresses, Mater. Sci. Eng. A 283 (2000) 225–233, https://doi.org/10.1016/S0921-5093(00)00703-6.
[30] R.O. Ritchie, Mechanisms of fatigue crack propagation in metals, ceramics and composites: role of crack tip shielding, Mater. Sci. Eng. 103 (1988) 15–28, https://doi.org/10.1016/0025-5416(88)90547-2.
[31] P. Fratzl, Biomimetic materials research: what can we really learn from nature's structural materials? J. R. Soc. Interface 4 (2007) 637–642, https://doi.org/10.1098/rsif.2007.0218.
[32] M.E. Launey, R.O. Ritchie, On the fracture toughness of advanced materials, Adv. Mater. 21 (2009) 2103–2110, https://doi.org/10.1002/adma.200803322.
[33] H. Chai, D. Josell, Fracture behavior of nano-layered coatings under tension, Thin Solid Films 519 (2010) 331–336, https://doi.org/10.1016/j.tsf.2010.07.086.
[34] H. Wu, G. Fan, M. Huang, L. Geng, X. Cui, R. Chen, G. Peng, Fracture behavior and strain evolution of laminated composites, Compos. Struct. 163 (2017) 123–128, https://doi.org/10.1016/j.compstruct.2016.12.036.
[35] N.K. Simha, O. Kolednik, F.D. Fischer, Material force models for cracks - influences of eigenstrains, thermal strains & residual stresses, ICF XI - 11th Int. Conf. Fract. 2005 http://www.icf11.com/proceeding/EXTENDED/5329.pdf.
[36] A. Moridi, H. Ruan, L.C. Zhang, M. Liu, Residual stresses in thin film systems: effects of lattice mismatch, thermal mismatch and interface dislocations, Int. J. Solids Struct. 50 (2013) 3562–3569, https://doi.org/10.1016/j.ijsolstr.2013.06.022.
[37] M. Tkadletz, J. Keckes, N. Schalk, I. Krajinovic, M. Burghammer, C. Czettl, C. Mitterer, Residual stress gradients in α-Al 2 O 3 hard coatings determined by pencil-beam X-ray nanodiffraction: the influence of blasting media, Surf. Coat.

Technol. 262 (2015) 134–140, https://doi.org/10.1016/j.surfcoat.2014.12.028.
[38] M. Stefenelli, R. Daniel, W. Ecker, D. Kiener, J. Todt, A. Zeilinger, C. Mitterer, M. Burghammer, J. Keckes, X-ray nanodiffraction reveals stress distribution across an indented multilayered CrN-Cr thin film, Acta Mater. 85 (2015) 24–31, https://doi.org/10.1016/j.actamat.2014.11.011.
[39] M. Deluca, R. Hammer, J. Keckes, J. Kraft, F. Schrank, J. Todt, O. Robach, J.-S. Micha, S. Defregger, Integrated experimental and computational approach for residual stress investigation near through-silicon vias, J. Appl. Phys. 120 (2016) 195104, , https://doi.org/10.1063/1.4967927.
[40] X. Song, K.B. Yeap, J. Zhu, J. Belnoue, M. Sebastiani, E. Bemporad, K. Zeng, A.M. Korsunsky, Residual stress measurement in thin films at sub-micron scale using Focused Ion Beam milling and imaging, Thin Solid Films 520 (2012) 2073–2076, https://doi.org/10.1016/j.tsf.2011.10.211.
[41] A.M. Korsunsky, M. Sebastiani, E. Bemporad, Residual stress evaluation at the micrometer scale: analysis of thin coatings by FIB milling and digital image correlation, Surf. Coat. Technol. 205 (2010) 2393–2403, https://doi.org/10.1016/j.surfcoat.2010.09.033.
[42] M. Krottenthaler, C. Schmid, J. Schaufler, K. Durst, M. Göken, A simple method for residual stress measurements in thin films by means of focused ion beam milling and digital image correlation, Surf. Coat. Technol. 215 (2013) 247–252, https://doi.org/10.1016/j.surfcoat.2012.08.095.
[43] D. Vogel, E. Auerswald, J. Auersperg, P. Bayat, R.D. Rodriguez, D.R.T. Zahn, S. Rzepka, B. Michel, Stress analyses of high spatial resolution on TSV and BEoL structures, Microelectron. Reliab. 54 (2014) 1963–1968, https://doi.org/10.1016/j.microrel.2014.07.098.
[44] S. Massl, J. Keckes, R. Pippan, A direct method of determining complex depth profiles of residual stresses in thin films on a nanoscale, Acta Mater. 55 (2007) 4835–4844, https://doi.org/10.1016/j.actamat.2007.05.002.
[45] R. Bermejo, Y. Torres, A.J. Sanchez-Herencia, C. Baudin, M. Anglada, L. Llanes, Residual stresses, strength and toughness of laminates with different layer thickness ratios, Acta Mater. 54 (2006) 4745–4757, https://doi.org/10.1016/j.actamat.2006.06.008.
[46] X.B. Ren, Z.L. Zhang, B. Nyhus, Effect of residual stresses on ductile crack growth resistance, Eng. Fract. Mech. 77 (2010) 1325–1337, https://doi.org/10.1016/j.engfracmech.2010.03.007.
[47] L. Náhlík, L. Šestáková, P. Hutař, R. Bermejo, Prediction of crack propagation in layered ceramics with strong interfaces, Eng. Fract. Mech. 77 (2010) 2192–2199, https://doi.org/10.1016/j.engfracmech.2010.02.023.
[48] M. Lugovy, V. Slyunyayev, V. Subbotin, N. Orlovskaya, G. Gogotsi, Crack arrest in Si3N4-based layered composites with residual stress, Compos. Sci. Technol. 64 (2004) 1947–1957, https://doi.org/10.1016/j.compscitech.2004.02.007.
[49] M. Rakin, O. Kolednik, B. Medjo, N.K. Simha, F.D. Fischer, A case study on the effect of thermal residual stresses on the crack-driving force in linear-elastic bimaterials, Int. J. Mech. Sci. 51 (2009) 531–540, https://doi.org/10.1016/j.ijmecsci.2009.05.006.
[50] M. Rakin, O. Kolednik, N.K. Simha, F.D. Fischer, Influence of residual stresses on the crack driving force in bimaterials with sharp interface, ICF XI - 11th Int. Conf. Fract. 2005 http://www.icf11.com/proceeding/EXTENDED/4457.pdf.
[51] J.D. Eshelby, J.M. Ball, D. Kinderlehrer, P. Podio-Guidugli, M. Slemrod (Eds.), Energy Relations and the Energy-Momentum Tensor in Continuum Mechanics BT - Fundamental Contributions to the Continuum Theory of Evolving Phase Interfaces in Solids: A Collection of Reprints of 14 Seminal Papers, Springer Berlin Heidelberg, Berlin, Heidelberg, 1999, pp. 82–119, , https://doi.org/10.1007/978-3-642-59938-5_5.
[52] M.E. Gurtin, Configurational Forces as Basic Concepts of Continuum Physics, 1st ed., Springer-Verlag, New York, 2000, https://doi.org/10.1007/b97847.
[53] G.A. Maugin, Configurational Forces: Thermodynamics, Physics, Mathematics, and Numerics, CRC Press Inc, 2010.
[54] O. Kolednik, R. Schöngrundner, F.D. Fischer, A new view on J-integrals in elastic–plastic materials, Int. J. Fract. 187 (2014) 77–107, https://doi.org/10.1007/s10704-013-9920-6.
[55] J.R. Rice, A path independent integral and the approximate analysis of strain concentration by Notches and Cracks, J. Appl. Mech. 35 (1968) 379–386, https://doi.org/10.1115/1.3601206.
[56] N.K. Simha, F.D. Fischer, G.X. Shan, C.R. Chen, O. Kolednik, J-integral and crack driving force in elastic-plastic materials, J. Mech. Phys. Solids 56 (2008) 2876–2895, https://doi.org/10.1016/j.jmps.2008.04.003.
[57] C.R. Chen, J. Pascual, F.D. Fischer, O. Kolednik, R. Danzer, Prediction of the fracture toughness of a ceramic multilayer composite - Modeling and experiments, Acta Mater. 55 (2007) 409–421, https://doi.org/10.1016/j.actamat.2006.07.046.
[58] R. Treml, D. Kozic, J. Zechner, X. Maeder, B. Sartory, H.P. Gänser, R. Schöngrundner, J. Michler, R. Brunner, D. Kiener, High resolution determination of local residual stress gradients in single- and multilayer thin film systems, Acta Mater. 103 (2016) 616–623.
[59] R. Schöngrundner, R. Treml, T. Antretter, D. Kozic, W. Ecker, D. Kiener, R. Brunner, Critical assessment of the determination of residual stress profiles in thin films by means of the ion beam layer removal method, Thin Solid Films 564 (2014) 321–330.
[60] R. Treml, D. Kozic, R. Schöngrundner, O. Kolednik, H.-P. Gänser, R. Brunner, D. Kiener, Miniaturized fracture experiments to determine the toughness of individual films in a multilayer system, Extrem. Mech. Lett. 8 (2016) 235–244, https://doi.org/10.1016/j.eml.2016.01.004.
[61] R. Mueller, S. Kolling, D. Gross, On configurational forces in the context of the finite element method, Int. J. Numer. Methods Eng. 53 (2002) 1557–1574, https://doi.org/10.1002/nme.351.
[62] R. Mueller, D. Gross, G.A. Maugin, Use of material forces in adaptive finite element methods, Comput. Mech. 33 (2004) 421–434, https://doi.org/10.1007/s00466-003-0543-z.
[63] A. Riedl, R. Daniel, M. Stefenelli, T. Schöberl, O. Kolednik, C. Mitterer, J. Keckes, A novel approach for determining fracture toughness of hard coatings on the micrometer scale, Scr. Mater. 67 (2012) 708–711, https://doi.org/10.1016/j.scriptamat.2012.06.034.
[64] T.L. Anderson, Fracture Mechanics: Fundamentals and Applications, 3rd ed., CRC Press Inc, 2005.
[65] M. Sistaninia, O. Kolednik, Effect of a single soft interlayer on the crack driving force, Eng. Fract. Mech. 130 (2014) 21–41, https://doi.org/10.1016/j.engfracmech.2014.02.026.
[66] B.N. Jaya, V. Jayaram, Fracture testing at small-length scales: from plasticity in Si to brittleness in Pt, JOM 68 (2016) 94–108, https://doi.org/10.1007/s11837-015-1489-2.